https://doi.org/10.1016/j.apacoust.2019.107071

Development of thin sound absorber by parameter optimization of multilayer compressed porous metal with rear cavity

Xinmin Shen[a, b, *], Panfeng Bai[b], Liang Chen[b], Sandy To[a, *], Fei Yang[b], Xiaonan Zhang[b], Qin Yin[b]

[a]State Key Laboratory in Ultra-precision Machining Technology, Department of Industrial and Systems Engineering, The Hong Kong Polytechnic University, Kowloon, Hong Kong, China;

[b]Department of Mechanical Engineering, College of Field Engineering, Army Engineering University, Nanjing, Jiangsu, China.

Corresponding author: shenxmjfjlgdx2014@163.com; sandy.to@polyu.edu.hk

Abstract. Practicability and applicability of the sound absorber can be improved by reducing its total thickness, and thin sound absorber was developed by optimizing the multilayer compressed porous metal with the rear cavity in this research. Theoretical model of sound absorption coefficient of the multilayer compressed porous metal with the rear cavity was constructed through the transfer matrix method based on Johnson-Champoux-Allard model, and its structural parameters were optimized to obtain optimal average sound absorption coefficient in 100-6000 Hz by the cuckoo search algorithm. Finite element simulation of the sound absorbers was conducted in the virtual acoustic laboratory for preliminary verification. According to the optimal structural parameters, single compressed porous metals were prepared and assembled to the optimal multilayer compressed porous metal with the rear cavity, and their sound absorption coefficients in 100-6000 Hz were measured according to standing wave method. Through the theoretical modeling, parameter optimization, finite element simulation, and standing wave tube measurement, an effective and practical sound absorber with actual average sound absorption coefficient of 0.5105 was developed by optimal 4-layer compressed porous metal with the total thickness of 5 mm, which would promote its application in the noise reduction field.

Keywords: thin sound absorber; multilayer compressed porous metal; parameter optimization; cuckoo search algorithm; finite element simulation; standing wave tube measurement.

1. Introduction

The growing problem of noise pollution has attracted more and more attentions [1], which results in enormous potential demand of the sound absorbing materials [2, 3]. Sound absorption properties of the sound absorbing material are mainly decided by its structural parameters [4]. Generally speaking, increasing total thickness of the sound absorbing material is considered as the most effective method to achieve the better sound absorption performance [5]. However, along with the rapid developments of miniaturization, integration, and portability of the precision components, the available installation space for sound absorbing material is strictly limited in lower range, which raise the new challenge to develop the novel sound absorber with simultaneous high sound absorption performance and thin total thickness [6]. Meanwhile, reducing total thickness of the sound absorber can not only decrease its occupied space, but also reduce the costs in its transport, installation, maintenance, replacement, and recycling [7], which are favorable for its practical application and sustainable development.

Some sound absorbing materials have been investigated to develop thin sound absorber [8-12]. Wang et al. [8] had proposed the porous metal fiber materials with gradient structure with the thickness of 2-3 mm, and average sound absorption coefficient of the 2-layer gradient structure with the porosity levels of 58.2% + 76.4% could reach 0.1007 in the frequency of 50-6400 Hz. The 3D reticular nickel foam and its composite structure were investigated on sound absorption in the frequency of 200-2000 Hz by Cheng et al. [9], and sound absorption coefficient of the composite structure of 5-layer foam (1-layer thickness: 2.3 mm) with a rear 5 mm-thick cavity could reach 0.4 in the 1000-1600 Hz. Besides these traditional sound absorbing materials, some acoustic metamaterials with thin thickness were also developed [10-12]. Li and Assouar [10] had developed acoustic metasurface-based perfect absorber with deep subwavelength thickness by combining the perforated plate and coiled coplanar

air chamber, which could achieve the total absorption at 125.8 Hz. The ultra-thin metamaterial made of rigid panel with a periodic distribution of thin closed slits was proposed by Jimenez et al. [11], and perfect absorption of sound was achieved at 338.5 Hz with a panel thickness of 11 mm. Huang et al. [12] had presented the spiral metasurface composed of the coiled channel and embedded aperture, which could obtain perfect absorption at the 146.75 Hz, 158 Hz, and 168 Hz when the corresponding thickness was 24 mm, 21.5 mm, and 20 mm respectively. However, major advantage of the acoustic metamaterial is achievement of the perfect absorption at certain low frequency point, and its normal absorption band is small. Moreover, the complex shape and delicate structure of the present acoustic metamaterial indicate that its fabrication cost is high, which limits its practical application. Therefore, development of the novel sound absorber with thin total thickness from traditional sound absorbing materials is still considered as the effective method at present.

It has been proved that sound absorption efficiency of the porous metal can be effectively improved through the compression and combination [13-16], which provide a potential way to develop novel thin sound absorber from the common porous metal. Bai et al. [13] had investigated influences of the compression ratio on sound absorption performance of porous nickel-iron alloy, which preliminarily studied and validated effect of the compression on sound absorption performance of the porous metal. The high-efficiency and thin-thickness acoustic absorber of gradient compressed porous metal was proposed by Yang et al. [14], which investigated influence of the permutations of single compressed porous metal and the optimal average sound absorption coefficient of 0.6033 in the 100-6000 Hz was obtained with the thickness of 11 mm. Yang et al. [15] had further developed the 10-layer gradient compressed porous metal with the limited thickness of 20 mm, average sound absorption coefficients of which reached 0.3325, 0.5412, 0.7461, and 0.7617 when the investigated frequency ranges were

100-1000 Hz, 100-2000 Hz, 100-4000 Hz, and 100-6000 Hz, respectively. Furthermore, it had been proved by Bai et al. [16] that the compressed porous metal with rear cavity could obtain excellent sound absorption, and average sound absorption coefficients of the single-layer compressed porous metal (the compression ratio was 0.9) were 0.3669, 0.5108, 0.5597, and 0.5714 when lengths of the rear cavity were 5 mm, 10 mm, 15 mm, and 20 mm, respectively. Therefore, design and optimization of the multilayer compressed porous metal with rear cavity were conducted in this research.

For this study, in order to reduce influence of a motor to other precise instruments in the vehicle, the average sound absorption coefficient in 100-6000 Hz should exceed 0.4, and the available space to install the sound absorber was limited to 5 mm. Theoretical model of sound absorption coefficient of the multilayer compressed porous metal with layer number of 1 to 5 was constructed through transfer matrix method [17, 18] based on the Johnson-Champoux-Allard model [19, 20]. Afterwards, average sound absorption coefficients of the proposed sound absorbers were optimized by the cuckoo search algorithm [21-23] through selecting the appropriate structural parameters. Preliminary verifications of the theoretical optimal sound absorbers were conducted according to the finite element simulation in virtual acoustic laboratory [24], which aimed to improve efficiency of the parameter optimization, reduce cost of the sample preparation, and decrease time of the experimental measurement. After that, the selected optimal sound absorbers were prepared by compression and combination of the porous metal samples according to the optimal structural parameters, and their sound absorption coefficients were measured according to the standing wave method [25, 26], which were treated as experimental validation to the theoretical sound absorbing model, cuckoo search optimization algorithm, and finite element simulation analysis. Finally, the optimization effect and formation cause of the proposed thin sound absorbers were analyzed based on their morphology characterization.

2. Theoretical modeling

The proposed thin sound absorber consisted of multilayer compressed porous metal and cavity, and its sound absorption coefficient could be theoretically modeled through transfer matrix method [17, 18] based on Johnson-Champoux-Allard model [19, 20]. Supposing layer number of the multilayer compressed porous metal was n, the corresponding transfer matrix P_i of the i^{th} $(1 \le i \le n)$ layer compressed porous metal could be calculated according to the Johnson-Champoux-Allard model [19, 20], as shown in the Eq. (1). Here k_i is the wave number in the i^{th} layer compressed porous metal, which can be derived by the Eq. (2); d_i is thickness of the i^{th} layer compressed porous metal, which can be obtained by the Eq. (3); Z_i is characteristic impedance of the i^{th} layer compressed porous metal, which can be obtained by the Eq. (4); j is symbol of the imaginary number.

$$P_i = \begin{bmatrix} \cos(k_i d_i) & jZ_i \sin(k_i d_i) \\ jZ_i^{-1} \sin(k_i d_i) & \cos(k_i d_i) \end{bmatrix} \tag{1}$$

$$k_i = \omega \sqrt{\frac{\rho_i(\omega)}{K_i(\omega)}} \tag{2}$$

$$d_i = d_0 \cdot (1 - \eta_i) \tag{3}$$

$$Z_i = \sqrt{\rho_i(\omega) K_i(\omega)} \tag{4}$$

In the Eqs. (2) and (4), ω is the sound angular frequency, which can be calculated from the acoustic frequency f by the Eq. (5); $\rho_i(\omega)$ is complex effective density of the i^{th} layer compressed porous metal, which can be derived by the Eq. (6); $K_i(\omega)$ is complex effective bulk modulus of the i^{th} layer compressed porous metal, which can be obtained by the Eq. (7). In the Eq. (3), d_0 is thickness of the original porous metal before compression, which can be measured by vernier caliper; η_i is compression ratio of the i^{th} layer compressed porous metal, which is defined as the ratio of the reduced thickness by the compression to original thickness of the porous metal [13-16].

$$\omega = 2\pi f \tag{5}$$

$$\rho_i(\omega) = \rho\left[1+\left(3^2+\frac{4\omega\rho}{\sigma_i\phi_i}\right)^{-0.5} - j\frac{\sigma_i\phi_i}{\omega\rho}\left(1+\frac{\omega\rho}{4\sigma_i\phi_i}\right)^{0.5}\right] \tag{6}$$

$$K_i(\omega) = \gamma P_0\left[\gamma-(\gamma-1)\left(1-N_u\left(j\frac{8\omega\rho P_r}{\sigma_i\phi_i}+N_u\right)^{-1}\right)\right]^{-1} \tag{7}$$

In the Eqs. (6) and (7), ρ is density of the air under normal condition, 1.21 Kg/m^3; σ_i is static flow resistivity of the i^{th} layer compressed porous metal, which can be calculated by the Eq. (8); ϕ_i is porosity of the i^{th} layer compressed porous metal, which can be obtained by the Eq. (9); γ is specific heat ratio of the air, 1.40; P_0 is standard static pressure of the air under normal condition, $1.013\cdot10^5$ Pa; N_u is the Nusselt number, 4.36; P_r is the Prandtl number, 0.71 [13-16, 19, 20].

$$\sigma_i = \frac{\phi_0}{(\phi_0-\eta_i)(1-\eta_i)}\sigma_0 \tag{8}$$

$$\phi_i = \frac{\phi_0-\eta_i}{1-\eta_i} \tag{9}$$

In the Eqs. (8) and (9), σ_0 is static flow resistivity of the original porous metal before compression, which can be calculated by the Eq. (10) based on the water tank method [27]; ϕ_0 is porosity of the original porous metal, which can be calculated by the Eq. (11) according to its definition [28].

$$\sigma_0 = \frac{\Delta p}{\upsilon d_0} \tag{10}$$

$$\phi_0 = \left(1-\frac{M}{V}\cdot\frac{1}{\rho_1}\right)\cdot100\% \tag{11}$$

In the Eq. (10), Δp is the pressure difference between front surface and back surface of the porous metal; υ is velocity of the air flow in the porous metal; d_0 is thickness of the porous metal. In the Eq. (11), M is mass of the porous metal, which can be measured by the electronic balance; V is volume of the porous metal, which can be calculated through measuring its size and thickness by the

vernier caliper; ρ_1 is density of the metal, which can be measured by the drainage method [29]. Meanwhile, transfer matrix S of the cavity back the multilayer compressed porous metal can be calculated by the Eq. (12). Here D is length of the cavity; c is the acoustic velocity in air under normal condition, 340 m/s. According to the transfer matrix method [17, 18], total transfer matrix T of the proposed sound absorber, which consisted of the n-layer compressed porous metal and the rear cavity, can be calculated by the Eq. (13), and the corresponding sound absorbing coefficient α can be derived by the Eq. (14). Here $\mathrm{Re}(\ )$ and $\mathrm{Im}(\ )$ represent the real part and imaginary part of one complex number respectively.

$$S = \begin{bmatrix} \cos\left(\omega D c^{-1}\right) & j\rho c \sin\left(\omega D c^{-1}\right) \\ j\rho^{-1}c^{-1}\sin\left(\omega D c^{-1}\right) & \cos\left(\omega D c^{-1}\right) \end{bmatrix} \tag{12}$$

$$T = \begin{bmatrix} T_{11} & T_{12} \\ T_{21} & T_{22} \end{bmatrix} = \prod_{i=1}^{n} P_i \cdot S \tag{13}$$

$$\alpha = \frac{4\,\mathrm{Re}\left(\frac{T_{11}}{T_{21}} \cdot \frac{1}{\rho c}\right)}{\left[1 + \mathrm{Re}\left(\frac{T_{11}}{T_{21}} \cdot \frac{1}{\rho c}\right)\right]^2 + \left[\mathrm{Im}\left(\frac{T_{11}}{T_{21}} \cdot \frac{1}{\rho c}\right)\right]^2} \tag{14}$$

Through the Eqs. (1) to (14), theoretical sound absorption coefficient of the proposed sound absorber could be obtained by putting the related parameters into the formulas, which supplied the theoretical basis and contrastive reference for the following structural parameter optimization, finite element simulation, sample preparation, and experimental measurement.

3. Parameter optimization

The used porous metal samples in this study were purchased from Yiyang Foam metal New material Co., Yiyang, Hunan, China, and their unified structural parameters of thickness d_0, porosity ϕ_0, and static flow resistivity σ_0 were 5 mm, 0.95, and 9524 Pa·s/m^2, respectively. Therefore, for this study,

sound absorption performance of the multilayer compressed porous metal with the rear cavity were determined by compression ratio η_i of each layer and length of the cavity D. Taking the research object in this study into consideration, there were two constraint conditions. Firstly, total thickness of the proposed sound absorber should be smaller than 5 mm, as shown in the Eq. (15). Secondly, it had been validated by the compression experiments that the compression ratio η_i should be smaller than 0.9 for the utilized porous metal samples in this research [14, 15], as shown in the Eq. (16), because structures of the compressed porous metal samples were more and more dense, and there would be almost no compressible space when the compression ratio was close to 0.95 (porosity of the original porous metal sample). Meanwhile, the optimization target was to obtain the maximal average sound absorption coefficient in the frequency of 100-6000 Hz, as shown in the Eq. (17).

$$\sum_{i=1}^{n} d_i + D \le 5 \cdot 10^{-3} \tag{15}$$

$$\eta_i < 0.9 \tag{16}$$

$$\max\left(average\left(\alpha(f)\right), f \in [100, 6000]\right) \tag{17}$$

According to the constructed theoretical sound absorbing model in Eqs. (1) to (14), the summarized constraint conditions in the Eqs. (15) and (16), and the given optimization target in the Eq. (17), parameter optimization of the proposed sound absorber, which consisted of multilayer compressed porous metal and rear cavity, was conducted according to the cuckoo search algorithm [21-23], and flow chart of the optimization process was shown in Fig. 1. For each investigated sound absorber, n groups of the solutions for parameters of the multilayer compressed porous metal with the rear cavity were randomly generated, and the objective function was defined by using the constructed theoretical sound absorbing model, the given optimization target, and the listed constraint conditions. Besides, maximum discovery probability and maximum iteration number were setup to initialize the cuckoo

search program. Through iterative computations of the objective values and continuous update of the superior solutions, the final optimal solution of the parameters could be achieved. In particular, for a certain pending optimized parameter of x_i, update of the new generation solution $x_i^{(t+1)}$ from the present generation solution $x_i^{(t)}$ was realized according to the Levy flight [21-23, 30], as shown in the Eq. (18). Here β is the step size, which should be related to scales of the problem of interests and $\beta = O(1)$ can be used in many cases [22]; Levy distribution of $Levy(s,\lambda)$ is the step length, as shown in the Eq. (19), which has an infinite variance with an infinite mean. In the Eq. (19), s is the step size drawn from a Levy distribution [21, 22].

$$x_i^{(t+1)} = x_i^{(t)} + \beta \oplus Levy(s,\lambda) \tag{18}$$

$$Levy(s,\lambda) \sim s^{-\lambda}, (\lambda \in (1,3]) \tag{19}$$

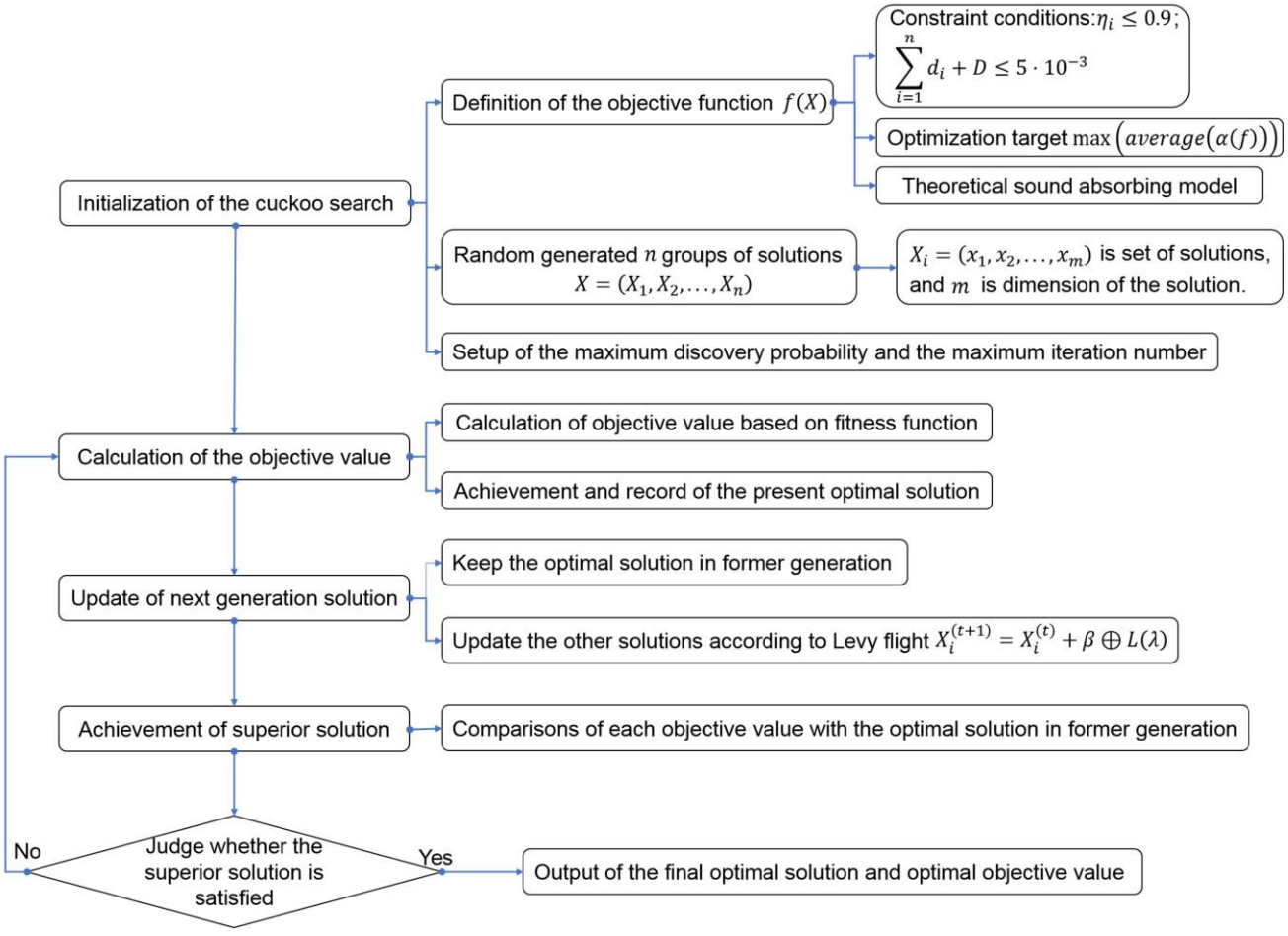

Fig. 1 Flow chart of the cuckoo search optimization program.

The obtained optimal structural parameters for the multilayer compressed porous metal with the rear cavity were summarized in Table 1, and the average sound absorption coefficients in the 100-6000 Hz were 0.2710, 0.3541, 0.4096, 0.4376, and 0.4461 when the layer numbers were 1-5. It could be found that the proposed sound absorbers could meet the requirement that average sound absorption coefficient exceeded 0.4 when the layer numbers were 3, 4, and 5. Meanwhile, it could be observed that improvement of the average sound absorption coefficient was reduced along with the increase of layer number, which indicated that there was no sense to further raise the layer number.

Table 1. Summarized optimal parameters of multilayer compressed porous metal with the rear cavity.

Sound absorber	1^{st} layer	2^{nd} layer	3^{rd} layer	4^{th} layer	5^{th} layer	Cavity (mm)	Average sound absorption coefficient
1-layer compressed porous metal with the rear cavity	0.9	-	-	-	-	4.5	0.2710
2-layer compressed porous metal with the rear cavity	0.9	0.47	-	-	-	1.8	0.3541
3-layer compressed porous metal with the rear cavity	0.9	0.57	0.53	-	-	0	0.4096
4-layer compressed porous metal with the rear cavity	0.9	0.89	0.60	0.62	-	0	0.4376
5-layer compressed porous metal with the rear cavity	0.9	0.89	0.69	0.74	0.78	0	0.4461

Distributions of the sound absorption coefficients of the optimal multilayer compressed porous metal with the rear cavity were shown in the Fig. 2, and the original porous metal without compression was treated as contrast. Average sound absorption coefficient of the original porous metal with thickness of 5 mm was 0.1163, which proved that the sound absorption performance was improved remarkably by parameter optimization of the multilayer compressed porous metal with the rear cavity, especially in the 1000-6000 Hz. Meanwhile, it could be found that sound absorption coefficients of the 5-layer compressed porous metal were close to those of the 4-layer compressed porous metal, which was

consistent with the results in Table 1 and further proved that it was unnecessary to simply improve the layer number. Furthermore, increase of the layer number meant to use more materials and raise weight of the sound absorber, which indicated that there would be an appropriate layer number.

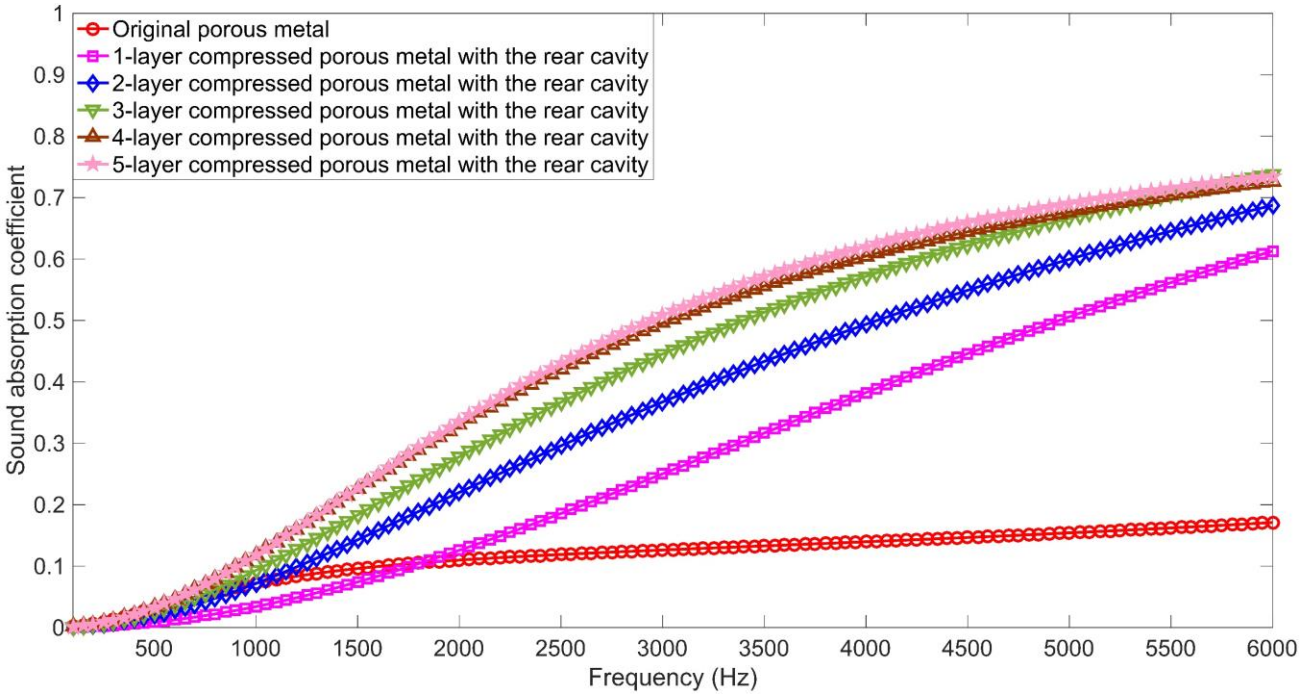

Fig. 2 Distributions of sound absorption coefficients of the optimal multilayer compressed porous metal with the rear cavity obtained by cuckoo search algorithm.

4. Finite element simulation

Finite element simulation model for the investigated sound absorber was constructed in the virtual acoustic laboratory, as shown in the Fig. 3, which was considered as preliminary verifications of the theoretical optimal sound absorbers. Size of the standing wave tube in the finite element simulation model was 60 mm × 60 mm × 300 mm, and the plane wave was loaded in the acoustic source inlet as the incidental wave. The sound absorber was installed in the end of the standing wave tube, and its thickness was 5 mm in this study. Two microphones were fixed on the standing wave tube, and their distances to the sound absorber were 90 mm and 50 mm respectively. Sound absorption coefficient of the sound absorber was calculated by the measured acoustic pressures at the two microphones, as

shown in Eq. (20). Here p_1 is the acoustic pressure at microphone 1; p_2 is the acoustic pressure at microphone 2; k_0 is the wave number; s is the distance between the two microphones, 40 mm; x_l is the distance between the microphone 1 and surface of the measured sound absorber, 90 mm.

$$\alpha=1-\left|\frac{\frac{p_2}{p_1}-e^{-jk_0s}}{e^{jk_0s}-\frac{p_2}{p_1}}\cdot e^{j2k_0x_l}\right|^2 \tag{20}$$

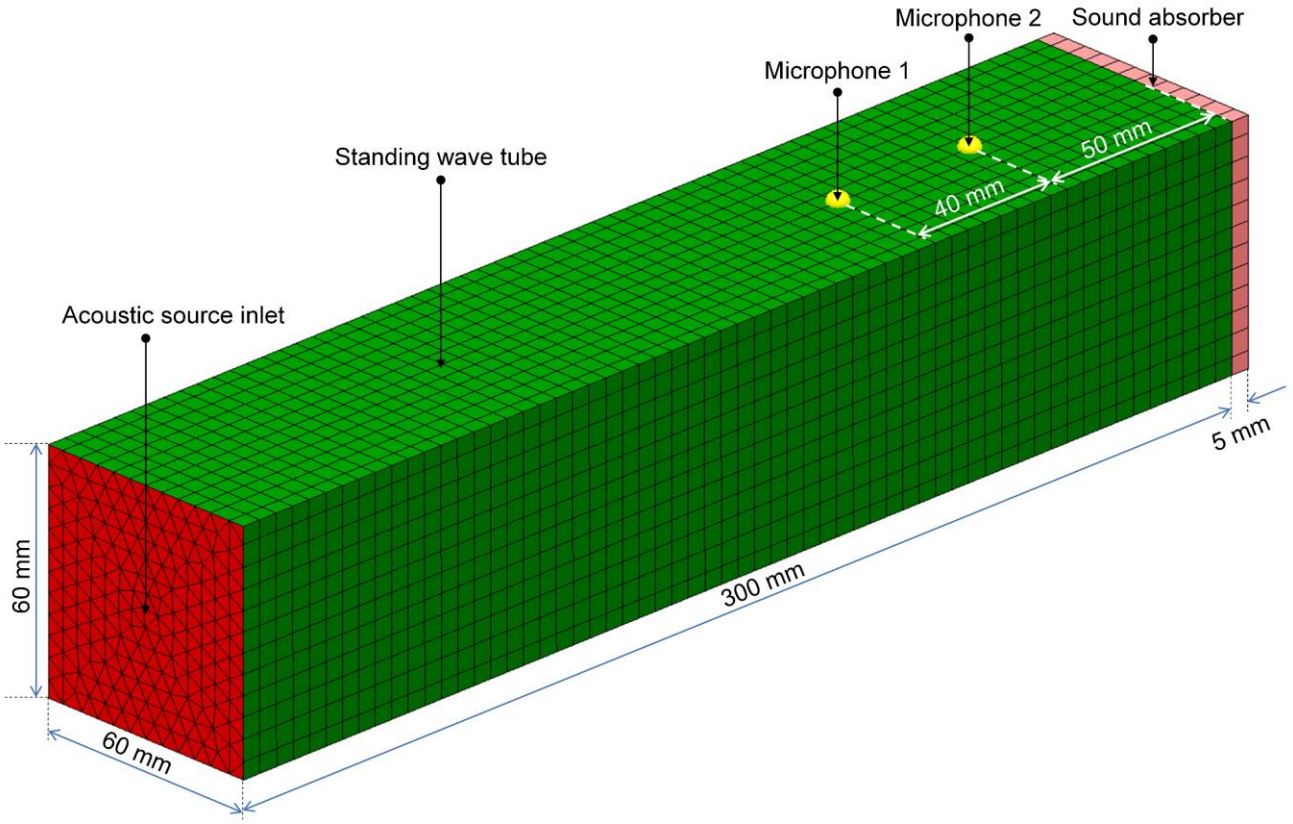

Fig. 3 Finite element simulation model for sound absorption coefficient of the sound absorber.

Schematic drawing compositions of finite element model for the investigated sound absorbers were shown in Fig. 4, and the colors were used to distinguish the different layers and the cavity. shape of the mesh in the finite element simulation model was frontal triangle, and its size was set to 5 mm. thickness of each layer and length of the cavity were consistent with the obtained optimal parameters for the proposed multilayer compressed porous metal with the rear cavity in the Table 1. In this way, sound absorption performances of the investigated sound absorbers were simulated.

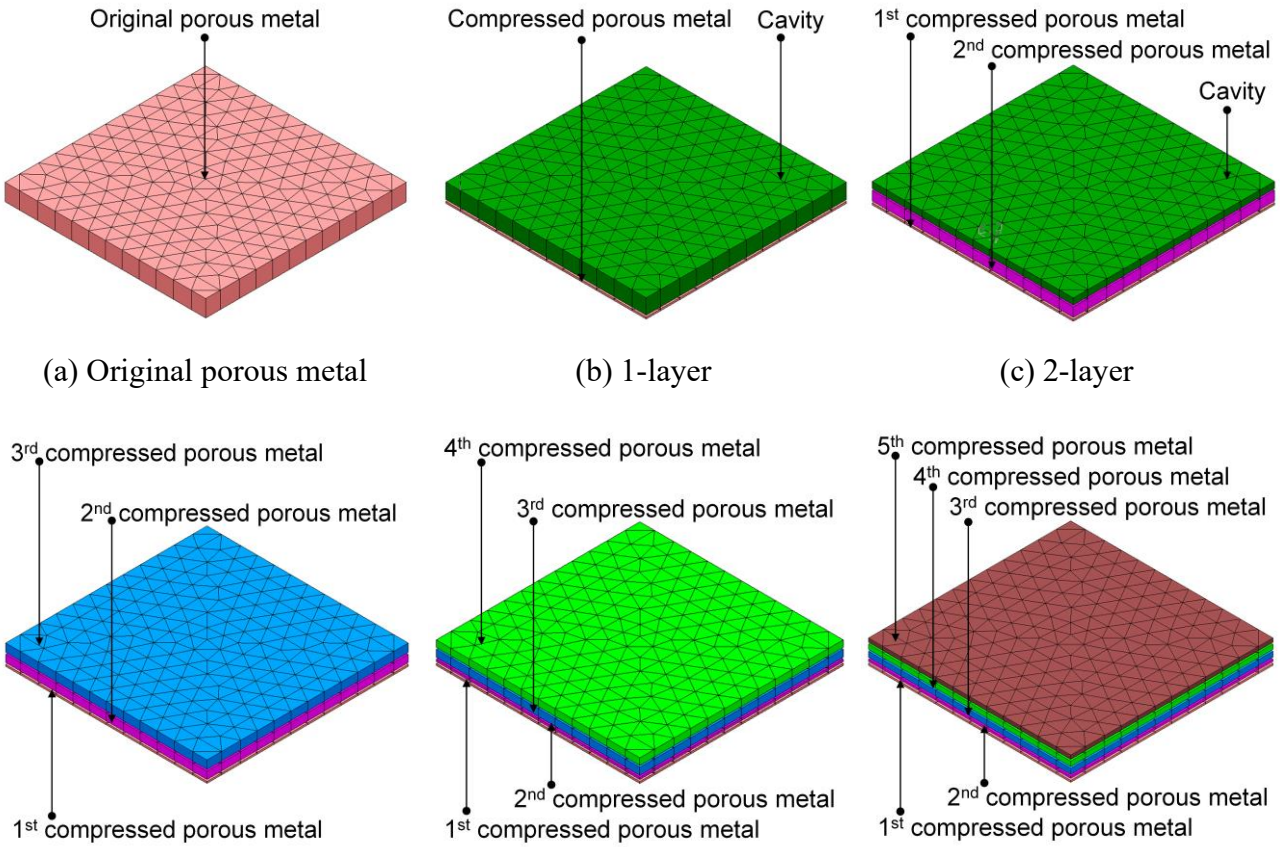

(a) Original porous metal (b) 1-layer (c) 2-layer

(d) 3-layer (e) 4-layer (f) 5-layer

Fig. 4 Schematic drawing compositions of finite element model for the investigated sound absorbers.

Comparisons of sound absorption coefficients of the investigated sound absorber in theory and those in simulation were shown in the Fig. 5. It could be observed that the simulation data were consistent with the theoretical data for each sound absorber, which preliminary verified efficiency and accuracy of parameter optimization of multilayer compressed porous metal with the rear cavity. There were two major reasons for the differences between simulation data and theoretical data. Firstly, the model for the porous metal was Johnson-Champoux-Allard model in the theoretical modeling process [19, 20], and that was Delany-Bazley-Miki model [31, 32] in the finite element simulation. Secondly, the used way to calculate the sound absorption coefficient in the theoretical model was transfer matrix method [17, 18], and that in finite element simulation was standing wave method [25, 26]. Although there were slight differences between the theoretical data and the simulation data, the finite element

simulation could be treated as an effective way for rapid verification of the sound absorber.

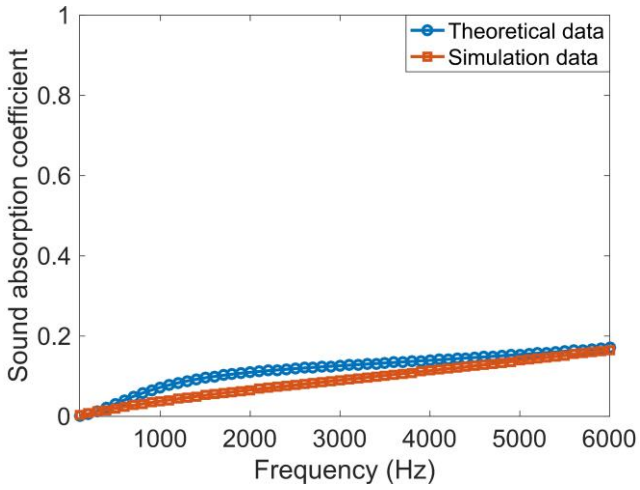

(a) Original porous metal

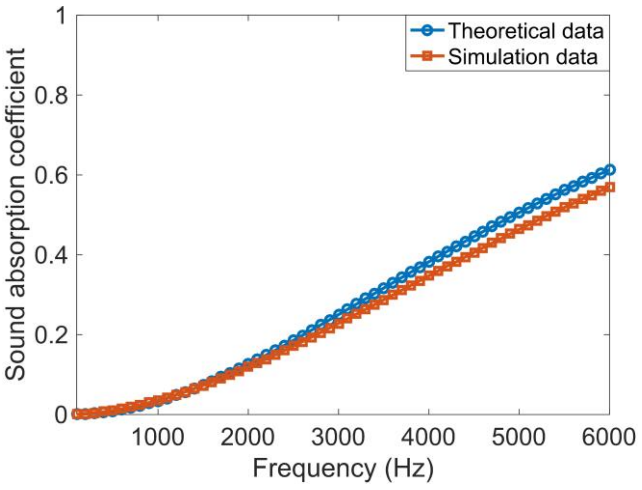

(b) 1-layer compressed porous metal

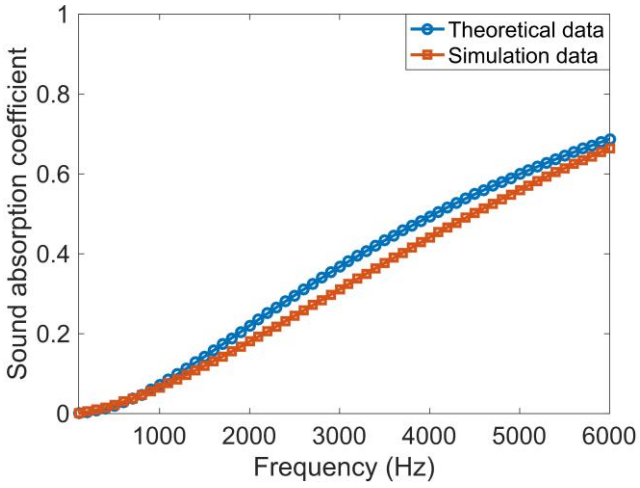

(c) 2-layer compressed porous metal

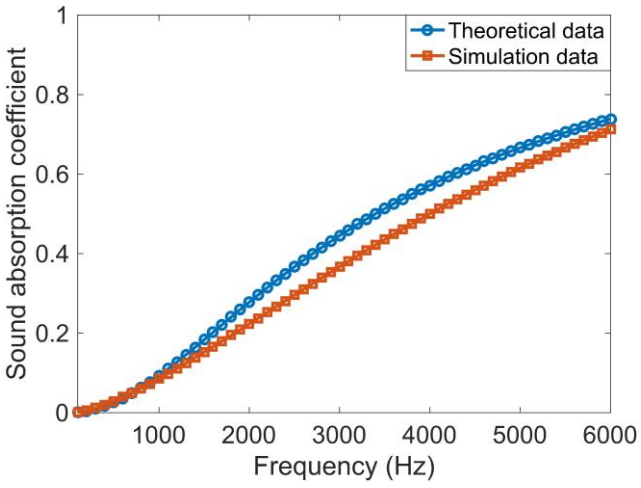

(d) 3-layer compressed porous metal

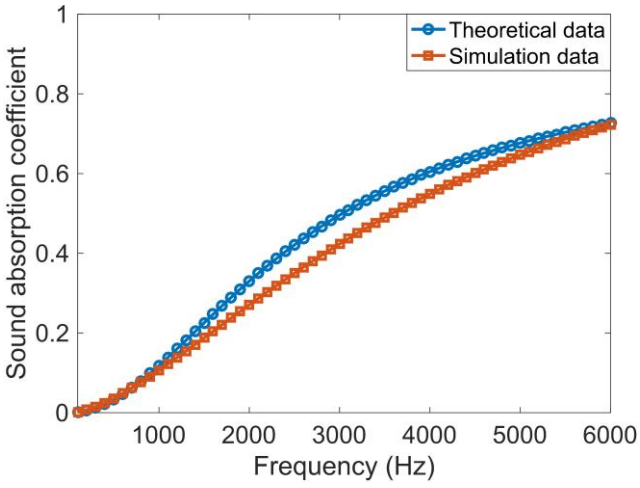

(e) 4-layer compressed porous metal

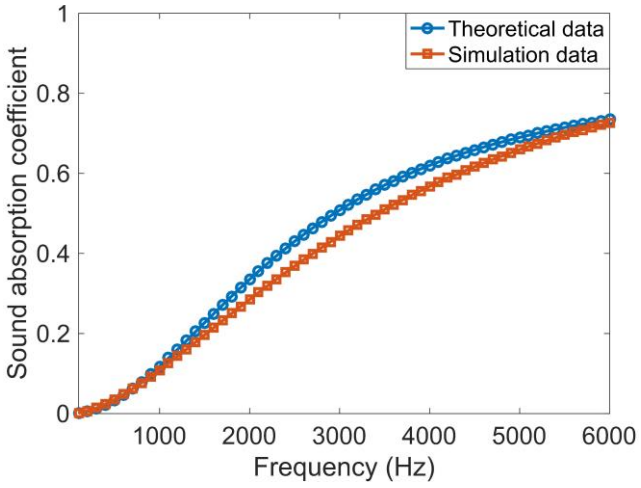

(f) 5-layer compressed porous metal

Fig. 5 Verification of absorption performance of the sound absorbers by finite element simulation.

5. Sample preparation

Each single compressed porous metal sample for the optimal multilayer compressed porous metal with the rear cavity was prepared by the CTM2050 universal testing machine (Wuxi City Bleecker Trading Co., Ltd., Wuxi, Jiangsu, China) [14] according to the obtained structural parameter in Table 1. The original porous metal sample was placed on the lower plate, and the standard block made of high-strength steel was used to ensure residual thickness of the compressed porous metal. In order to avoid the elastic deformation in compression of the porous metal, the compression force was set as 10 KN and the compression process continued for 10 min [14, 15].

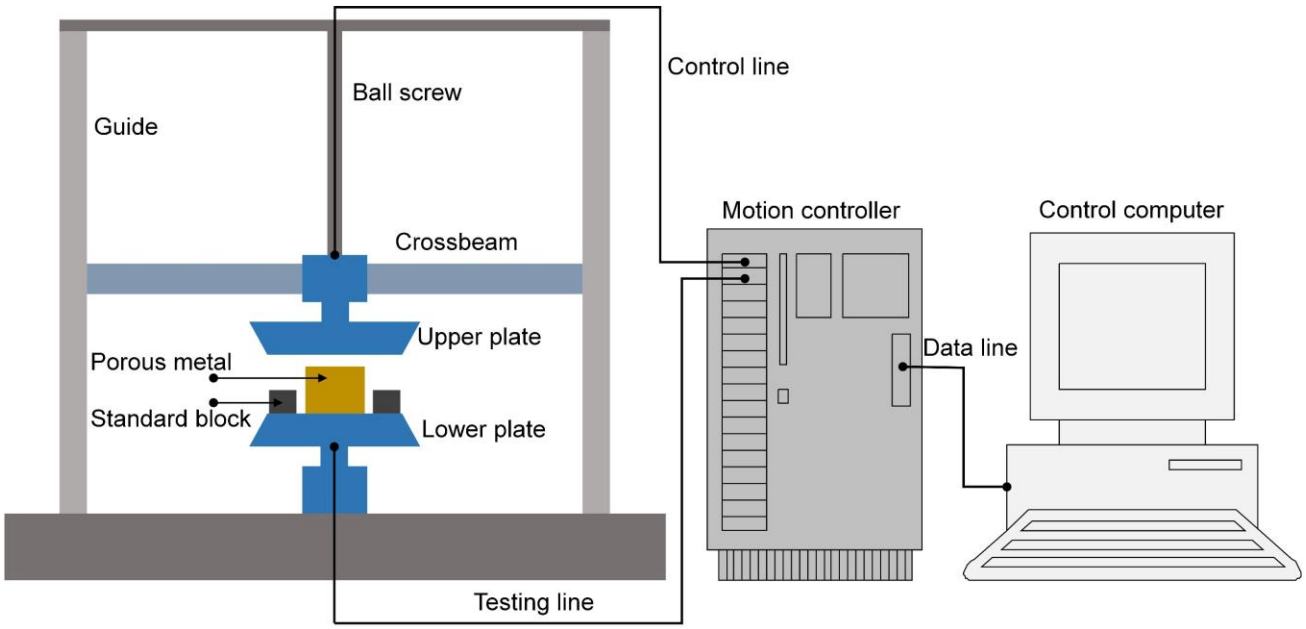

Fig. 6 Schematic diagram of CTM2050 universal testing machine for compression of porous metal.

The prepared samples of multilayer compressed porous metal and original porous metal were shown in Fig. 7. In order to satisfy requirement of further standing wave tube measurement, there were two samples for each sound absorber. The bigger one with the diameter of 96 mm was for measuring the sound absorption coefficient in the 100-2000 Hz, and the smaller one with the diameter of 30 mm was for measuring the sound absorption coefficient in the 2000-6000 Hz [13-16].

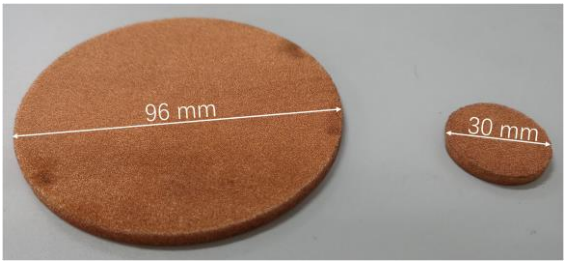

(a) Original porous metal

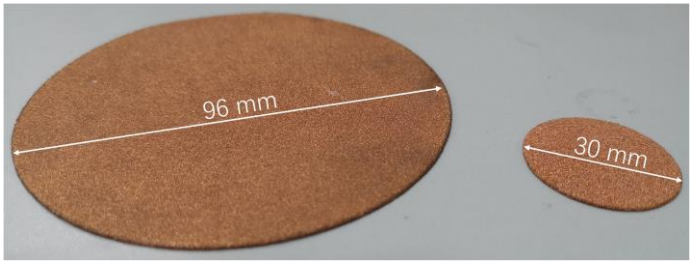

(b) 1-layer compressed porous metal

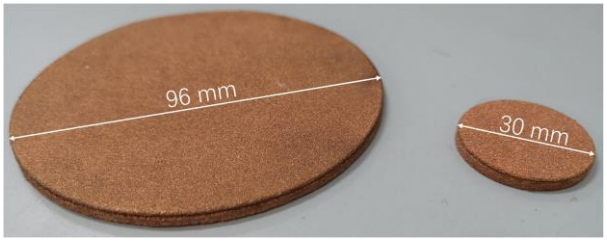

(c) 2-layer compressed porous metal

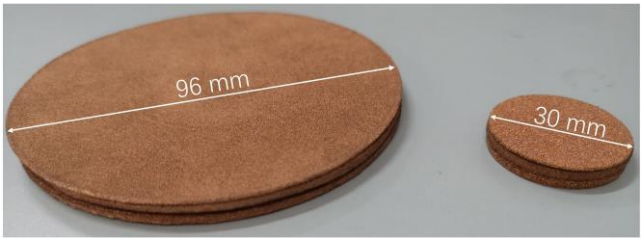

(d) 3-layer compressed porous metal

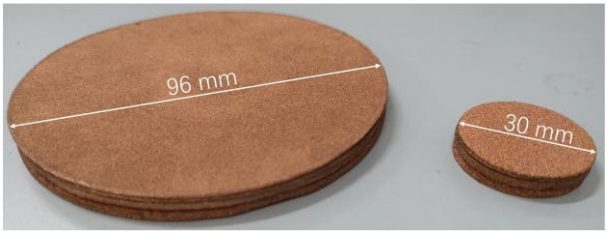

(e) 4-layer compressed porous metal

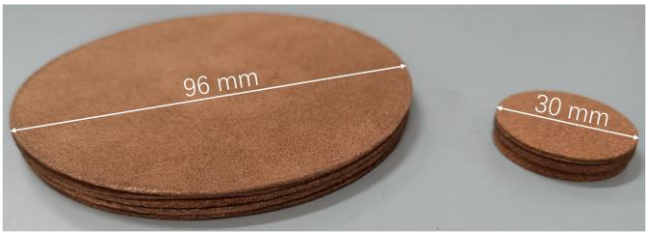

(f) 5-layer compressed porous metal

Fig. 7. The prepared samples of multilayer compressed porous metal and original porous metal.

6. Experimental measurement

The prepared multilayer compressed porous metal and original porous metal were measured by the AWA6128A detector (Hangzhou Aihua Instruments Co., Ltd., Hangzhou, Zhejiang, China) according to the standing wave method [25, 26], and its schematic diagram was shown in Fig. 8. The prepared sound absorber was placed into the sample fixer, and the rear cavity was controlled by the cavity adjuster. Total thickness of the multilayer compressed porous metal and the cavity was limited to 5 mm. the incidental wave was generated by the loudspeaker and input in the standing wave tube, and the reflected wave was received by the acoustic probe and transferred to the workstation. Through achievement of peak and valley acoustic pressure of the reflected wave by adjusting the pulley on the

slideway, sound absorption coefficient of the investigated sound absorber was obtained. In order to reduce the measurement error, each sound absorber was measured for 10 times, and the final sound absorption coefficients were average value of the 10 actual measured values.

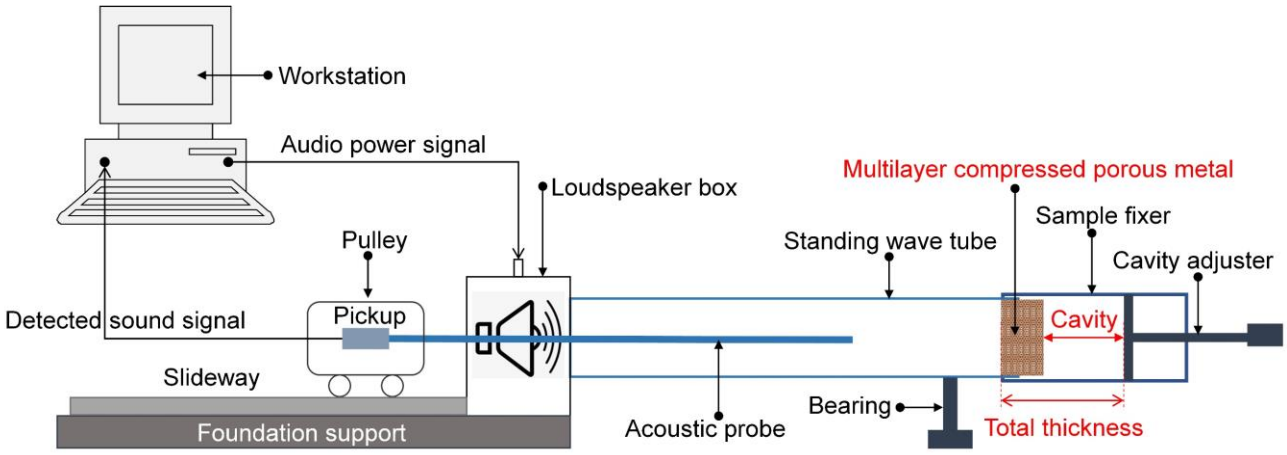

Fig. 8 Schematic diagram of AWA6128A detector for measurement of sound absorption coefficient.

After the standing wave tube measurement, comparisons of the theoretical data, simulation data, and experimental data of sound absorption coefficients of the investigated sound absorbers were shown in the Fig. 9. It could be observed that consistencies among the theoretical data, simulation data, and experimental data were good, especially in the low frequency range of 100-2000 Hz, which further validated the effectiveness and practicability of the theoretical sound absorbing model, cuckoo search optimization algorithm, and finite element simulation analysis. Meanwhile, it could be observed that there were obvious differences among the theoretical data, simulation data, and experimental data in the high frequency range of 4000-6000 Hz for the multilayer compressed porous metal with the rear cavity. The major reason for this phenomenon was that the porous structures were treated as polygon in the theoretical model and in the finite element simulation, and structural parameters of the single compressed porous metal were derived from porosity and static flow resistivity of the original porous metal and the compressed ratio [15]. These assumption and derivation were idealization of the actual situation, which led to deviations among the theoretical data, simulation data, and experimental data.

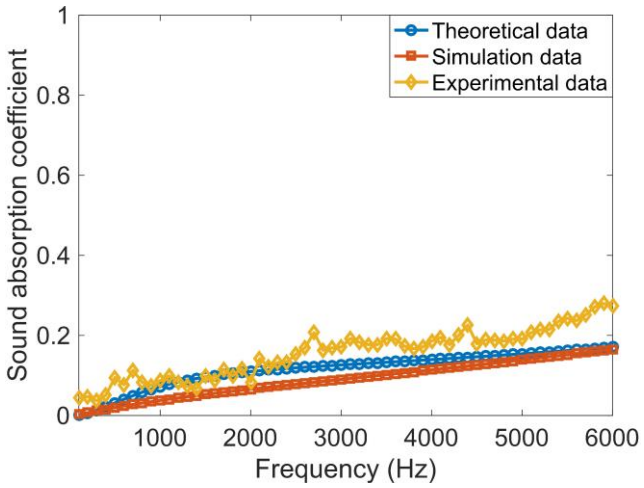

(a) Original porous metal

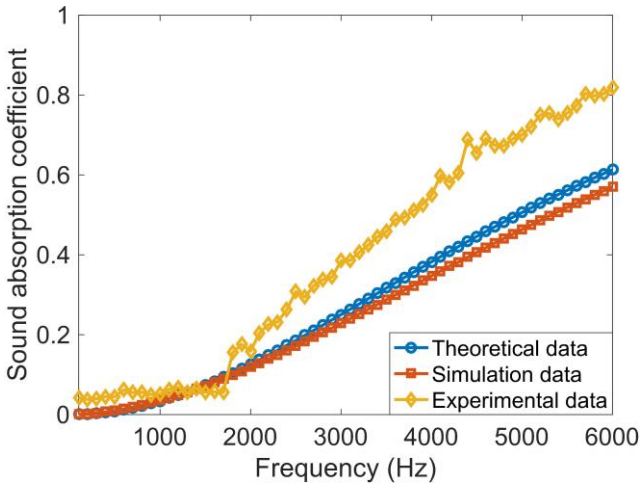

(b) 1-layer compressed porous metal

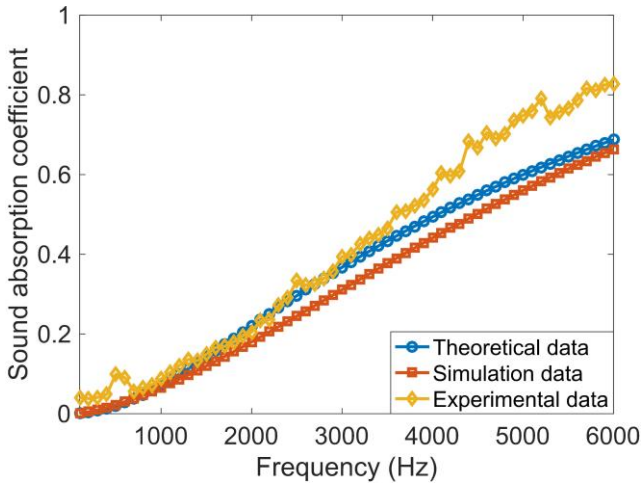

(c) 2-layer compressed porous metal

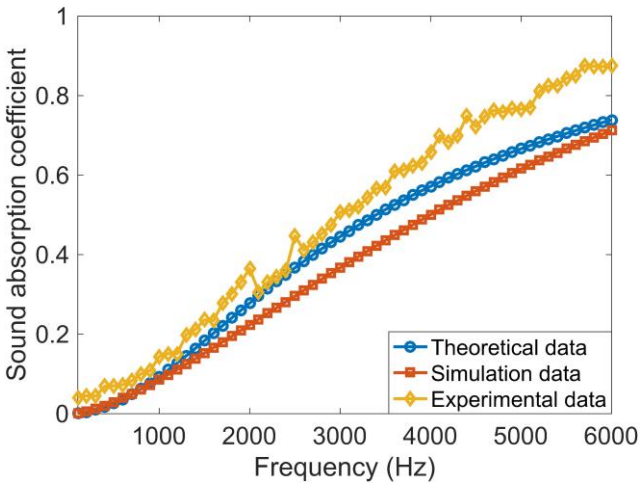

(d) 3-layer compressed porous metal

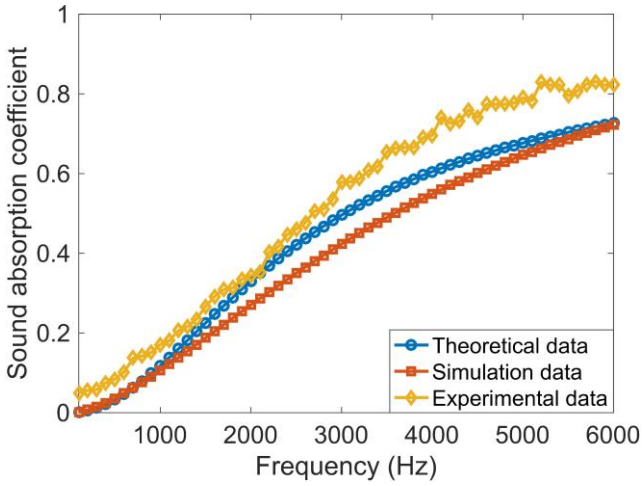

(e) 4-layer compressed porous metal

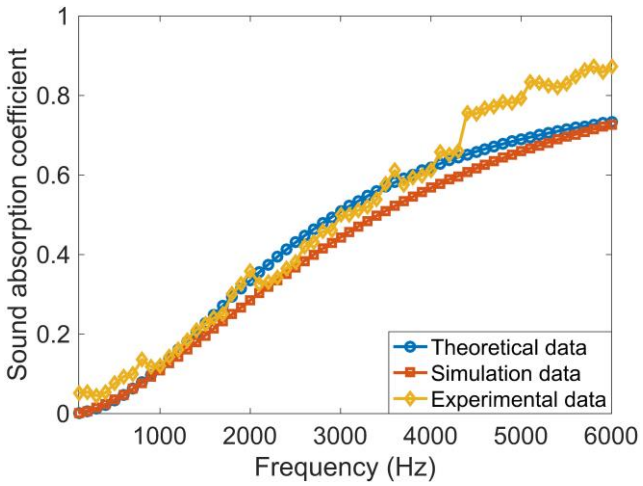

(f) 5-layer compressed porous metal

Fig. 9 Comparisons of sound absorption coefficients in theory, in simulation, and in experiment.

7. Results and discussion

The calculated average sound absorption coefficients of the investigated sound absorbers in theory, in simulation, and in experiment were summarized in the Table 2. It could be observed that for each sound absorber, the average sound absorption coefficient in experiment was significantly larger than that in theory and that in simulation, which could also be estimated and judged from comparisons of the sound absorption coefficients in the Fig. 9. Meanwhile, relative to the average sound absorption coefficient of 0.1581 for the original porous metal, the average sound absorption coefficient of the multilayer compressed porous metal with rear cavity was improved by more than 2 times. Especially when the layer numbers were 3, 4, and 5, the average sound absorption coefficient was improved by more than 3 times, which proved the effectiveness to develop the thin sound absorber by parameter optimization of the multilayer compressed porous metal with the rear cavity. Furthermore, it could be found that when layer number of the multilayer compressed porous metal reached or exceeded 2, the actual average sound absorption coefficient was over 0.4 in the 100-6000 Hz, which could meet the requirement of noise reduction for the vehicle in this study. It was interesting to note that the best actual average sound absorption coefficient of 0.5105 was obtained by optimal 4-layer compressed porous metal, instead of the optimal 5-layer compressed porous metal with cavity. The major reason for this phenomenon was supposed that excessive compression of the porous metal would reduce its sound absorption coefficient in the middle-high frequency range, which could also be judged from the experimental results in Fig. 9, because the porous structure was destroyed when the limited space was filled with the compressed porous metals with high compression ratio. Therefore, for the noise reduction of a motor in the vehicle in this research, the effective and practical sound absorber was developed by the optimal 4-layer compressed porous metal with the total thickness of 5 mm.

Table 2. Comparisons of average sound absorption coefficients of the investigated sound absorbers.

Sound absorbers	Average sound absorption coefficients		
	In theory	In simulation	In experiment
The original porous metal	0.1163	0.0897	0.1581
Optimal 1-layer compressed porous metal with rear cavity	0.2710	0.2496	0.3872
Optimal 2-layer compressed porous metal with rear cavity	0.3541	0.3193	0.4125
Optimal 3-layer compressed porous metal with rear cavity	0.4096	0.3630	0.4817
Optimal 4-layer compressed porous metal with rear cavity	0.4376	0.3985	0.5105
Optimal 5-layer compressed porous metal with rear cavity	0.4461	0.4105	0.4787

Comparisons of morphologies of the porous metal before and after the compression were shown in Fig. 10. It could be observed in Figs. 10(a) and 10(b) that the original porous metal consisted of the skeleton structures, which could obtain the sound absorption through the friction and viscous effects [19, 20]. The compression ratio for the compressed sample in Figs. 10(c) and 10(d) was 0.9. Judging from the surface and sectional morphologies, it could be found that the original porous structures were destroyed, and many irregular micro through-holes were generated in the compressed sample along the compression direction. Meanwhile, thickness of the compressed sample in Figs. 10(c) and 10(d) was 0.5 mm, which indicated that the resonance sound absorption effect could be realized by the micro through-holes like the microperforated panel absorber to some extent [14-16]. There was considered as the other reason for differences of the calculated average sound absorption coefficients obtained in theory, in simulation, and in experiment, because the resonance sound absorption effect of the micro through-holes in the compressed porous metal was not taken into consideration in the theoretical modeling process and finite element simulation analysis.

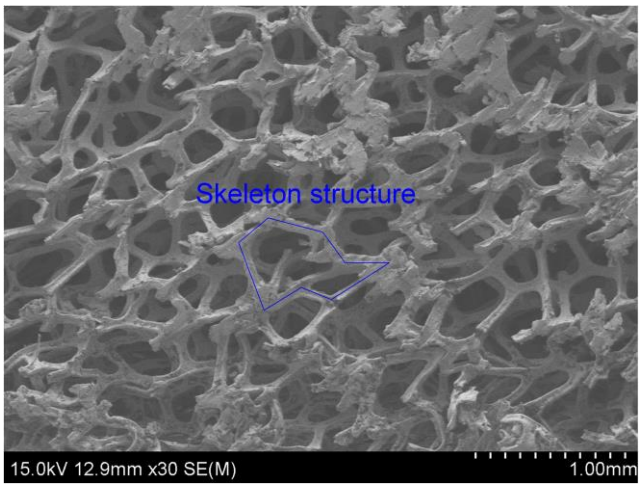

(a) Original sample with low magnification

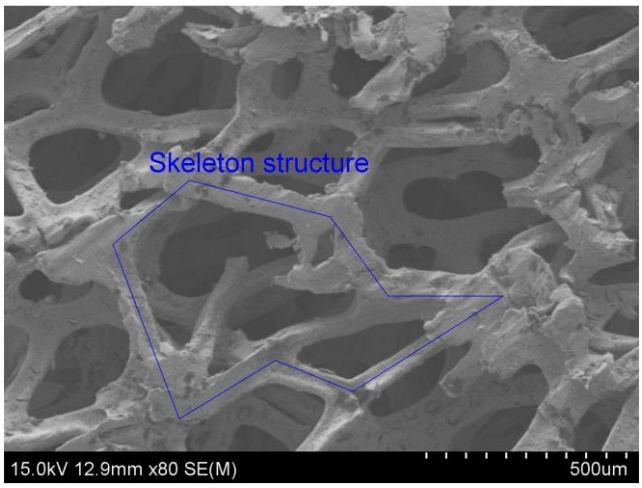

(b) Original sample with high magnification

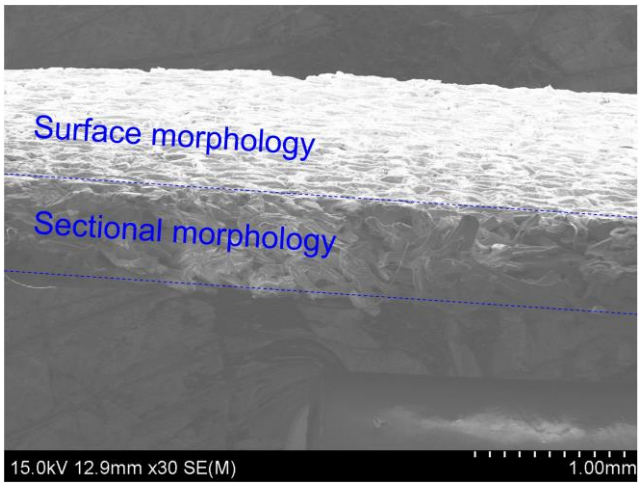

(c) Compressed sample with low magnification

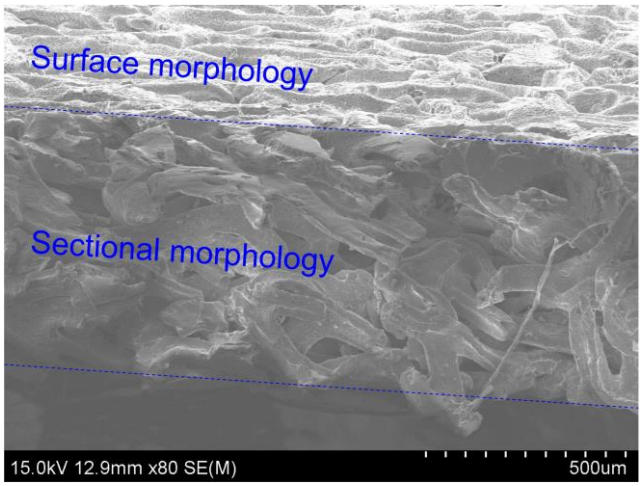

(d) Compressed sample with high magnification

Fig. 10 Comparisons of morphologies of the porous metal before and after the compression.

The layer-by-layer sectional morphologies of the 4-layer and 5-layer compressed porous metals were shown in Figs. 11 and 12 respectively, which aimed to investigate the difference between their sound absorption performances. As mentioned above, there existed resonance sound absorption effect in the multilayer compressed porous metal with the rear cavity. Therefore, relative to the 3rd and 4th layers of the 4-layer compressed porous metal in Figs. 11(b) and 11(c), 3rd, 4th, and 5th layers of the 5-layer compressed porous metal in Figs. 12(b) and 12(c) were more seriously compressed, which left fewer air spaces for the former 1st and 2nd layers. This was considered as the other reason for better sound

absorption performance of the optimal 4-layer compressed porous metal with the rear cavity.

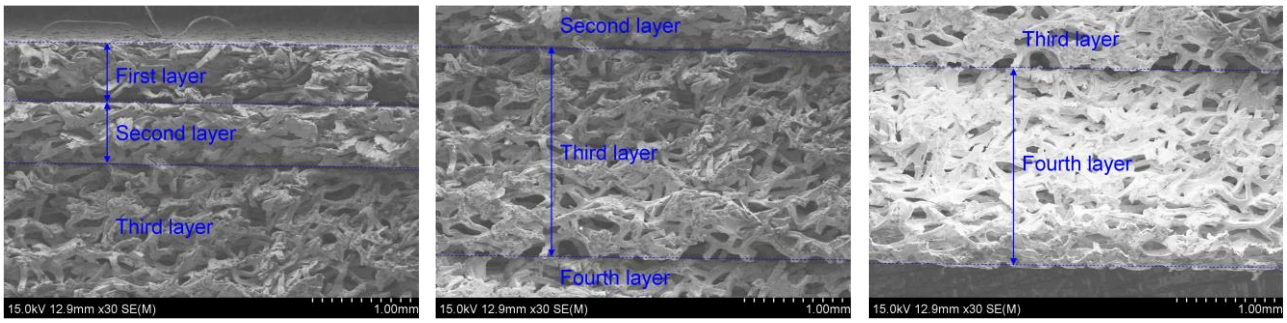

(a) 1st and 2nd layers (b) 3rd layer (c) 4th layer

Fig. 11 Layer-by-layer sectional morphologies of the 4-layer compressed porous metal.

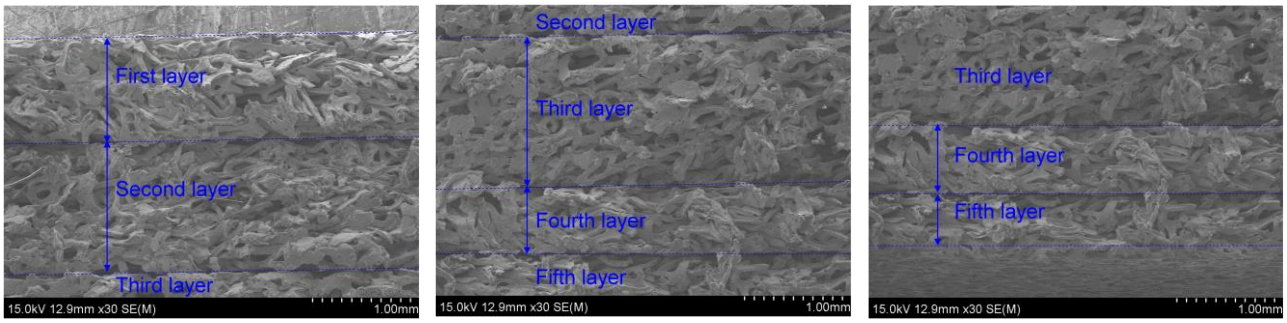

(a) 1st and 2nd layers (b) 3rd and 4th layers (c) 4th and 5th layers

Fig. 12 Layer-by-layer sectional morphologies of the 5-layer compressed porous metal.

8. Conclusions

The thin sound absorber obtained by parameter optimization of multilayer compressed porous metal with the rear cavity was proposed and developed in this research. Through the theoretical modeling, parameter optimization, finite element simulation, sample preparation, experimental measurement, and morphology characterization, the following conclusions were obtained.

(1) Relative to the actual average sound absorption coefficient of 0.1581 in the 100-6000 Hz for the original porous metal, it was improved to 0.3872, 0.4125, 0.4817, 0.5105, and 0.4787 for multilayer compressed porous metal with the rear cavity when layer number was 1-5 respectively. Improvement of the space utilization with limited total thickness and realization of the resonance sound absorption

effect by the micro through-holes were considered as two major occasions.

(2) The best actual average sound absorption coefficient of 0.5105 in the 100-6000 Hz was obtained by the optimal 4-layer compressed porous metal with the thin thickness of 5 mm, and the sequential compression ratios were 0.9, 0.89, 0.60, and 0.62 respectively for each layer. Extent of the damage of original pore structures and the residual air spaces for former layers were assumed as the two major occasions for different sound absorption performance of the multilayer compressed porous metal.

(3) Sound absorption coefficients of the multilayer compressed porous metal with the rear cavity in theory, in simulation, and in experiment were consistent, which validated effectiveness and accuracy of the theoretical sound absorbing model, cuckoo search optimization algorithm, and finite element simulation analysis. Idealization of the actual situation by assumption and without consideration of the resonance sound absorption effect in the theoretical modeling and finite element simulation were deemed as the two major reasons for the deviations among them three.

The developed sound absorber with the thin thickness of 5 mm and high average sound absorption coefficient of 0.5105 would be completely meet the requirement of noise reduction for the vehicle in this study. Meanwhile, this method was also effective to design and optimize the desired thin sound absorber for other conditions, which would be favorable to promote the application of porous metal in the noise reduction and perfect the sound absorption theory of porous material in the acoustics.

Acknowledgements

This work was supported by a grant from National Natural Science Foundation of China (Grant No. 51505498), a grant from Natural Science Foundation of Jiangsu Province (Grant No. BK20150714), and a grant from National Key R & D Program of China (Grant No. 2016YFC0802900). Xinmin Shen was grateful for support from the Hong Kong Scholars Program (No. XJ2017025).

References

[1] R.T. Buxton, M.F. McKenna, D. Mennitt, K. Fristrup, K. Crooks, L. Angeloni, G. Wittemyer, Science 356(6337) (2017) 531-533.

[2] U. Berardi, G. Iannace, Acoustic characterization of natural fibers for sound absorption applications, Build. Environ. 94(2) (2015) 840-852.

[3] M. Yang, P. Sheng, Sound Absorption Structures: From Porous Media to Acoustic Metamaterials, Annu. Rev. Mater. Res. 47 (2017) 83-114.

[4] M. Yang, S.Y. Chen, C.X. Fu, P. Sheng, Optimal sound-absorbing structures, Mater. Horiz. 4 (2017) 673-680.

[5] Z.Y. Lim, A. Putra, M.J.M. Nor, M.Y. Yaakob, Sound absorption performance of natural kenaf fibres, Appl. Acoust. 130 (2018) 107-114.

[6] J.L. Zhu, J. Sun, H.P. Tang, J.Z. Wang, Q.B. Ao, T.F. Bao, W.D. Song, Gradient-structural optimization of metal fiber porous materials for sound absorption, Powder. Technol. 301 (2016) 1235-1241.

[7] J.P. Arenas, M.J. Crocker, Recent trends in porous sound-absorbing materials, J. Sound. Vib. 44 (2010) 12-17.

[8] J.Z. Wang, Q.B. Ao, J. Ma, X.T. Kang, C. Wu, H.P. Tang, W.D. Song, Sound absorption performance of porous metal fiber materials with different structures, Appl. Acoust. 145 (2019) 431-438.

[9] W. Cheng, C.Y. Duan, P.S. Liu, M. Lu, Sound absorption performance of various nickel foam-base multi-layer structures in range of low frequency, Trans. Nonferrous Met. Soc. China 27(9) (2017) 1989-1995.

[10] Y. Li, B.M. Assouar, Acoustic metasurface-based perfect absorber with deep subwavelength thickness, Appl. Phys. Lett. 108(6) (2016) 063502.

[11] N. Jiménez, W. Huang, V. Romero-García, V. Pagneux, J.-P. Groby, Ultra-thin metamaterial for perfect and quasi-omnidirectional sound absorption, Appl. Phys. Lett. 109(12) (2016) 121902.

[12] S.B. Huang, X.S, Fang, X. Wang, B. Assouar, Q. Cheng, Y. Li, Acoustic perfect absorbers via spiral metasurfaces with embedded apertures, Appl. Phys. Lett. 113(23) (2018) 233501.

[13] P.F. Bai, X.M. Shen, X.N. Zhang, X.C. Yang, Q. Yin, A.X. Liu, Influences of compression ratio on sound absorption performance of porous nickel-iron alloy, Metals 8(7) (2018) 539.

[14] X.C. Yang, X.M. Shen, P.F. Bai, X.H. He, X.N. Zhang, Z.Z. Li, L. Chen, Q. Yin, Preparation and characterization of gradient compressed porous metal for high-efficiency and thin-thickness acoustic absorber, Materials 12(9) (2019) 1413.

[15] F. Yang, X.M. Shen, P.F. Bai, X.N. Zhang, Z.Z. Li, Q. Yin, Optimization and validation of sound absorption performance of 10-Layer gradient compressed porous metal, Metals 9(5) (2019) 588.

[16] P.F. Bai, X.C. Yang, X.M. Shen, X.N. Zhang, Z.Z. Li, Q. Yin, G.L. Jiang, F. Yang, Sound absorption performance of the acoustic absorber fabricated by compression and microperforation of the porous metal, Mater. Des. 167 (2019) 107637.

[17] K. Verdière, R. Panneton, S. Elkoun, T. Dupont, P. Leclaire, Transfer matrix method applied to the parallel assembly of sound absorbing materials, J. Acoust. Soc. Am. 134(6) (2013) 4648-4658.

[18] X.C. Yang, P.F. Bai, X.M. Shen, S. To, L. Chen, X.N. Zhang, Q. Yin, Optimal design and experimental validation of sound absorbing multilayer microperforated panel with constraint conditions, Appl. Acoust. 146 (2019) 334-344.

[19] N. Kino, Further investigations of empirical improvements to the Johnson-Champoux-Allard

model, Appl. Acoust. 96 (2015) 153-170.

[20] J.F. Allard, Y. Champoux, New empirical equations for sound propagation in rigid frame fibrous materials, J. Acoust. Soc. Am. 91(6) (1992) 3346-3353.

[21] X.S. Yang, S. Deb, Multiobjective cuckoo search for design optimization, Comput. Oper. Res. 40(6) (2013) 1616-1624.

[22] X.S. Yang, S. Deb, Cuckoo search: recent advances and applications, Neural. Comput. & Applic. 24(1) (2014) 169-174.

[23] X.M. Shen, P.F. Bai, X.C. Yang, X.N. Zhang, S. To, Low-frequency sound absorption by optimal combination structure of porous metal and microperforated panel, Appl. Sci. 9(7) (2019) 1507.

[24] M.-A. Gaudreau, F. Sgard, F. Laville, H. Nélisse, A finite element model to improve noise reduction based attenuation measurement of earmuffs in a directional sound field, Appl. Acoust. 119 (2017) 66-77.

[25] C. Bujoreanu, F. Nedeff, M. Benchea, M. Agop, Experimental and theoretical considerations on sound absorption performance of waste materials including the effect of backing plates, Appl. Acoust. 119 (2017) 88-93.

[26] X.C. Yang, K. Peng, X.M. Shen, X.N. Zhang, P.F. Bai, P.J. Xu, Geometrical and dimensional optimization of sound absorbing porous copper with cavity, Mater. Des. 131 (2017) 297-306.

[27] R.L. Brown, R.H. Bolt, The measurement of flow resistance of porous acoustic materials, J. Acoust. Soc. Am. 13(4) (1942) 337-344.

[28] F.Q. Tang, H. Fudouzi, T. Uchikoshi, Y. Sakka, Preparation of porous materials with controlled pore size and porosity, J. Eur. Ceram. Soc. 24(2) (2004) 341-344.

[29] J. Banhart, Manufacture, characterization and application of cellular metals and metal foams, Prog. Mater. Sci. 46(6) (2001) 559-632.

[30] A.H. Gandomi, X.S. Yang, A.H. Alavi, Cuckoo search algorithm: a metaheuristic approach to solve structural optimization problems, Eng. Comput.-Germany 29(1) (2013) 17-35.

[31] M.E. Delany, E.N. Bazley, Acoustical properties of fibrous absorbent materials, Appl. Acoust. 3(2) (1970) 105-116.

[32] Y. Miki, Acoustical properties of porous materials-Modifications of Delany-Bazley models, J. Acoust. Soc. Jpn. (E) 11(1) (1990) 19-24.